Modelling and Simulation of Industrial Multistage Flash Desalination Process with Exergetic and Thermodynamic Analysis. A case study of Azzour seawater desalination plant

A. H. Almerri [1], M. A. Al-Obaidi [2], S. Alsadaie [3] and I. M. Mujtaba [1, *]

[1] Department of Chemical Engineering, Faculty of Engineering and Informatics. University of Bradford. Bradford, West Yorkshire BD7 1DP, UK
[2] Middle Technical University, Technical Institute of Baquba, Dayala/Iraq
[3] Chemical Engineering Department, Faculty of Engineering, University of Sirte, Sirte/Libya
***Corresponding author, Tel.: +44 0 1274 233645**
E-mail address: I.M.Mujtaba@bradford.ac.uk

Abstract

Despite the fact of being intensive energy consumption, MSF is a mature technology that characterised by a high production capacity of high-quality water. The multistage flash (MSF) desalination process is one of the prominent thermal desalination used in the industry of seawater desalination to produce high quantity and high quality of freshwater. However, this process consumes large amount of energy and faces thermal limitations due to its high degree of exergy destruction at several units of the process. Therefore, the research of MSF is still existed to elevate the performance indicators and to resolve the concern of high energy consumption. To rectify these limitations, it is important to determine the units responsible in dissipating energy. This study aims to model an industrial MSF process validated against real data and then investigate the exergy destruction and thermodynamic limitations of the process. As a case study, Azzour MSF seawater desalination plant, located in Al Khiran in Kuwait is under the focus. A comprehensive model is developed by analysing several published models. Specifically, the calculation of exergy destruction has embedded both physical and chemical exergies that identified as a strong point of the model developed. As expected, the highest exergy destruction (55.5%) occurs within the heat recovery section followed by the brine heater with exergy destruction of 28.26% of the total exergy destruction. This study identifies the sections of the industrial process that cause the highest energy losses.

Keywords: Seawater desalination; Thermal technologies; Multistage flash; Modelling; Simulation; Thermodynamic analysis.

1. Introduction

Water is the absolute necessity for all leaving species including human being. In addition, water is by far the most important utility for all process industries. Although more than 70% of the world's surface is covered by water, only about 3% of total water is freshwater and was sufficient to meet the demand of freshwater (in every spheres of our life – domestic, agriculture to industries) for the last several decades. Hence, there was a need for converting abundant saline water into freshwater and commercial desalination plants have been continuously growing since fifties (Mujtaba et al., 2017; 2018; Buabbas et al., 2020). There are many thermal processes such as Multistage flash desalination, Multiple effect evaporation, vapour compressor, freeze desalination and humidification and dehumidification process that are applied in seawater desalination industry to produce freshwater from seawater resources. The well-known thermal processes are the Multistage Flash (MSF) desalination and Multiple Effect Evaporation (MEE) (Alasdair and Mujtaba, 2016; Al-hotmani et al., 2019). Current water supply market still places the thermal processes including multistage Flash (MSF) as a second process after Reverse Osmosis process to generate fresh water from seawater sources. Most Gulf Countries, including Saudi Arabia, Kuwait, UAE, Oman, Bahrain, and Qatar still choose thermal desalination as total or partial fresh water source.

Roughly a quarter of the plants use MSF distillation for its high product capacity with-high quality. However, the MSF process is considered as one of the most expensive desalination technologies that also produces high temperature waste. This is due to the need of the thermal and mechanical energy where it demands between 14 to 26 kWh/m^3 (Basile and Napporn, 2020). Due to the irreversibility of the MSF process, it is fair to expect a significant level of

energy dissipation that increases the specific energy consumption of the process and thus increases the unit production cost of the freshwater. In the past models of various complexity, from simple (El-dessouky and Ettouney, 2002) to detailed (Tanvir and Mujtaba, 2008; Alsadaie and Mujtaba, 2016) have been used to evaluate the performance of the process. However, many of these studies were not relevant to large scale industrial processes and have not included exergy and thermo-economic analysis which would improve the thermal efficiency of the process.

The distribution of energy resources of the system can be identified using the second law of thermodynamic. Thermo-economics distribute the expenses on the plant boundary in each unit streams based on the exergy not energy. The method of exergy analyses the plant losses and identifies the units causing losses based on mass and energy conservation principles together with the second law of thermodynamics (entropy equations) (Nafey et al., 2006a; Al-Weshahi et al., 2013; Fitzsimons et al., 2015). Ng et al. (2021) stated that the thermodynamic limitation for typical separation of water from the solution of 3.5% concentration by weight at ambient temperature and zero recovery is 0.78 kWh/m^3. However, the actual specific energy consumption for a typical seawater desalination process is around five to eight folds higher than the ideal thermodynamic limitation. Therefore, the efficiency of any thermal desalination system have to consider the actual ratio of output energy to input energy. In other words, the thermodynamic limitations and evaluating the energy losses is very important for the multistage flash (MSF) desalination plant to explore the level of deficiency and determine the most locations, streams and units that are responsible to dissipate the energy. Therefore, a high-fidelity process model is desirable to carry out exergy analysis accurately.

Limited numbers of studies can be found in the literature that focused on analysing the exergy of actual MSF seawater desalination plants. This is because of the associated complexity of determining the exergy based on a robust model. Al-Sulaiman and Ismail (1995) carried out

exergy analysis of 3 desalination plants of different sizes in Saudi-Arabia based on the plant data. The exergy destruction term and rate of exergy loss were found to be directly proportional to the top brine temperature of the process. There was no process model incorporating mass and energy balances and thermo-physical property evaluation correlations were based on several simplified assumptions.

Hamed et al. (2000) used a commercial computer program for MSF process simulation to analyse the thermal performance of six industrial desalination plants of varying features. Some of the operational data of these industries such as temperature, pressure, flow rate and salinity of these desalination plants were perhaps used as input data to the simulator used in the study. However, feature of the process model with associated assumptions of this commercial simulator were not discussed.

Kahraman and Cengel (2005) evaluated the exergy of a large-scale industrial MSF desalination process with capacity of 36,291 m^3/h of freshwater based on plant data. The low exergy efficiency of 4.2% confirmed the high possibility of improving the thermodynamic performance of the plant and reduce the exergy destruction. It was found that the exergy input was destroyed by 77.8%, 5.30% and 8.30% in the MSF stages, pump motors and brine heater, respectively. Accordingly, it was recommended that number of stages should be increased to reduce the exergy destruction. However, there was no process model incorporating mass and energy balances and thermo-physical property evaluation correlations used for this purpose.

Nafey et al. (2006b) considered a small capacity of MSF plant producing 209 m^3/hr of freshwater. The total exergy efficiency of 20 stages plant is 1.87% where the evaporators have the highest exergy destruction followed by the brine discharge stream and distillate stream. Also, the overall cost of the MSF plant can be reduced if the exergy destructions of the desuperheater and the distillate stream are reduced. The mathematical model considered by the authors included the money balance for each hardware component (boiler, turbine, pump etc.)

105 and several different set of auxiliary equations. However, they did not consider the model of
106 the distillation plant.
107 Abdulrahim and Alasfour (2010) considered multi-objective optimisation of hybrid MSF-RO
108 process where exergy destruction was calculated. The brine recycle MSF process was modelled
109 using a detailed MSF process model developed earlier by the authors. However, the study was
110 not aimed at any industrial desalination processes and lacked detailed investigation around
111 exergetic loss, efficiency etc.
112 Sharqawy et al. (2011) carried out the exergy analysis of the same industrial plant as was
113 considered by Kahraman and Cengel (2005) based on the same plant data. Sharqawy et al.
114 (2011) observed significant differences in exergy values compared to those obtained by
115 Kahraman and Cengel (2005) and attributed these differences to chemical exergy, which was
116 not considered by Kahraman and Cengel (2005) and due to use of different thermo-physical
117 property correlations.
118 Al-Weshahi et al. (2013) carried out exergy analysis of MSF seawater desalination plant of
119 3800 m^3/h of freshwater production. This study observed that around 54% of total exergy was
120 destructed in the heat recovery section. The study suggested that the heat from the hot distillate
121 water stages should be recovered to improve unit exergy efficiency. An off-the-shelf MSF
122 process simulator was used with published thermodynamic correlations of seawater. There was
123 no discussion on the details of the model with the associated assumptions in their paper.
124 Ghamdi and Mustafa (2016) investigated exergy of an industrial MSF process based on plant
125 data and a very simple model using MATLAB. The simulation indicated that increasing
126 number of heat recovery stages can decrease exergy destruction.
127 Most of the exergy calculations in the past were carried out for industrial MSF processes based
128 on plant data using simple to detailed thermodynamic properties evaluation correlations. There
129 was only one contribution where a simple MSF process model was used. Therefore, the focus

of this work is to develop a model-based platform for detailed exergy analysis of MSF desalination process using a comprehensive and realistic process model including reliable thermos-physical property evaluation correlations for carrying out exergetic calculations accurately. The overall model was coded in gPROMS software suits.

The model is validated fully with data from an industrial scale MSF desalination process which is Azzour MSF seawater desalination plant, located in Al Khiran in Kuwait. It consists of 24 stages (21 stages in the heat recovery section and 3 stages in the heat rejection section) with a capacity of 7570.8 m^3/h. We then use the validated MSF model to carry out the exergetic calculations. Note, as mentioned earlier, although there are several plants data-based exergy calculations, none of these studies considered exergetic analysis of the Azzour MSF plant. Our study focuses around improving the amount of electric and thermal energy supplied and to offer a cost-effective distillation method. More importantly, the calculation of total exergy has included the calculations of physical and chemical exergies, which has been neglected in most of the earlier work reported. This study aims to evaluate the exergy flow rates throughout all the components of the plant and discover the locations of major exergy destruction. This in turn would identify pathway to enhance energy efficiency in the Azzour MSF seawater desalination plant and attain a high-desalination performance at the lowest cost.

2. Description of the Azzour seawater MSF desalination plant

MSF process is a distillation process that extracts fresh water from high salinity water by converting amount of water into steam in multiple stages. The main design of the MSF unit consists of a brine heater and a series of flashing chambers work as heat exchangers. The heating source provides the unit with heat. This heat is enough to raise the seawater temperature to a desired temperature called top brine temperature (TBT). The hot seawater then enters a series of flashing chambers where the hot vapour starts to evaporate under a reduced pressure

process. The produced vapour is releasing its latent heat to the cooling seawater and converted into fresh liquid water and collected in distillate trays. The evaporation process is carried out in two sections, namely heat recovery section and heat rejection section. Typically, the heat rejection section consists of three flashing stages while the heat recovery section consists of several flashing stages (N stages) depends on the capacity of the plant. First, the heat is recovered from the flashing vapour in the heat recovery section. This is carried out via recovering the heat of vaporisation from high temperature flashing brine in the condensers. However, the heat rejection section is utilised to remove the extra heat added by the brine heater.

The MSF seawater desalination plant of Azzour (located in Al Khiran in Kuwait) has been designed as brine recycle layout MSF process as schematically plotted in Fig. 1. This design is specifically conducted to attain an increased performance ratio. The MSF plant contains three main parts of brine heater, heat recovery section and heat rejection section. The brine heater is the source of energy device that contains heat streams to heat the recycled brine stream from the heat rejection section. The flashing stages in heat rejection and heat recovery section are similarly designed. The Azzour desalination plant consists of 21 stages connected in a series in the heat recovery section and 3 stages connected in a series to form the heat rejection section. Specifically, increasing the number of stages above 20 stages would accommodate higher productivity and elevated performance ratio (Al-Fulaij, 2011). However, this would reduce the temperature difference between the flashing stage and upper condenser (driving force) and consequently this causes a reduction of thermal heat and requirement of growing the total heat transfer area of high cost.

The seawater treatment starts with feeding the seawater (cold stream) into the last stage in the heat rejection section to absorb the surplus heat and cool the distillate and high salinity brine. The recycled brine from the rejection stage is linked to a part of the disposed seawater and then

pumped within 7 bar and enters the last stage of the heat recovery section. In other words, the Azzour design comprises a recirculation of a determined portion of the cooling water leaving the heat rejection stage and back with the incoming cooling water to maintain approximately fixed temperature around of the cooling water at the entrance of the heat rejection stages as demonstrated in Fig. 1. This means a higher brine flow rate will be recycled to the heat recovery section compared to the original seawater flow rate fed to the plant. Specifically, the recirculated brine is designed to prevent low brine level in the corresponding flashing stages or flooding. The seawater enters the condenser tubes of stage 21 and then to stage 20 and so on until getting stage 1. This would increase seawater temperature and become within the designed top brine temperature before entering the brine heater to systematically enter the brine pool of the first stage with a designed top brine temperature. The steam of the brine heater is supplied to raise the seawater temperature to its top brine temperature where the seawater absorbs the latent heat of steam. Therefore, the brine is flashed inside the vacuum stage and introduces salt free vapour in the vapour phase and high salinity brine at the brine pool of the flashing stage. The vapour of the corresponding stage is directed to the condenser to produce distillate collected in a special tray. The vapours of all the stages are collected to form the main product stream while the brine of stage 24 represents the discharge stream to the sea (Fig. 1). The Azzour seawater desalination plant is supplied by proper venting system to reduce the contents of non-condensable gases (dissolved gases in water) that reduces the thermal heat efficiency with a high possibility of corrosion. Moreover, the Azzour plant is designed with demisters to decrease the brine droplets from the flashed off vapour. Again, this is an important device to maintain the process at the lowest scaling level on the surfaces of condensers and preheaters. Furthermore, the flow rate inside each stage is controlled via a brine orifice. Several pumps are also instilled in the MSF plant to guarantee proper pressure of the seawater or exiting streams

(product and discharged streams). The operating conditions and process design parameters of Azzour desalination plant are given in Table 1.

Table1. Actual operating conditions and design parameters of Azzour desalination plant (Adapted from Al-Shayji, 1998; Alasfour and Abdulrahim, 2009; Alsadaie, 2017)

Parameter	Unit	Value
Seawater flow rate	kg/s	2674.81
Seawater temperature	°C	35
Steam mass flow rate	kg/s	39.85
Steam temperature	°C	100
Recycle brine flow rate	kg/s	3968.33
Blow down brine flow rate	kg/s	497.55
Blow down temperature	°C	39.98
Makeup flow rate	kg/s	812.62
Top brine temperature	°C	90
Freshwater flow rate	kg/s	315.04
Freshwater temperature	°C	38.12
Parameter	**Heat rejection section**	**Heat recovery section**
Number of stages	3	21
Number of tubes bundle per stage	1588	1451
Heat transfer area	9444 m^2	77206 m^2
Brine heater: Heat transfer area	3544 m^2	

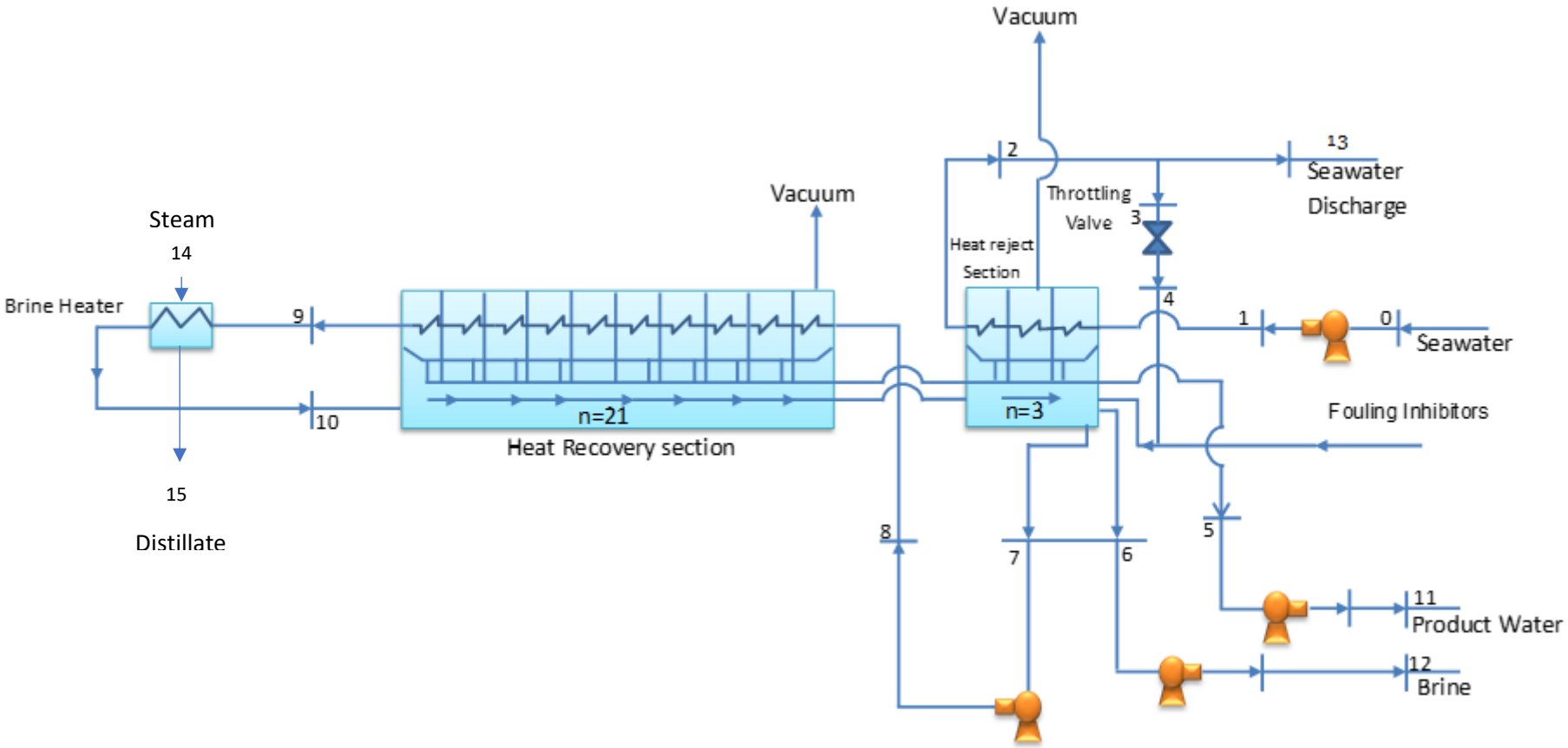

Fig. 1. Schematic diagram of the Azzour MSF seawater desalination plant and selected locations

3. Development of a comprehensive steady state model for MSF process

This section describes in detail the comprehensive steady state model developed to characterise the MSF desalination process that would combine two parts of models including the performance indicators prediction equations and thermodynamic limitations and exergy analysis equations. Therefore, the authors would confirm the gathering of these equations from literature to adequately deliver a comprehensive model for MSF system.

The full details of the sub models that form the comprehensive model of MSF process are presented in the next section.

3.1 Performance prediction model

The performance prediction model equations were constituted from different published models of Helal et al. (1986), Hussain et al. (1993), Rosso et al. (1997), El-Dessouky and Bingulac (1996), El-Dessouky et al. (1999), El-Dessouky and Ettouney (2002), Al-Fulaij et al. (2010), and Alsadaie (2017).

It is valuable to inform that the performance prediction model developed in this section has adopted functional relationships generated from total mass and material balance for MSF system. Moreover, the enthalpy balances that combined heat and mass transfer coefficients are also embedded. Furthermore, due to the expectation of varying the physical properties of seawater, the influence of temperature and seawater concentration on the physical properties are intensively included. The gPROMS software is used to code the model and carry out the main task of simulation.

3.1.1 Assumptions

For a complicated system, such MSF desalination system, it is necessary to state feasible model's assumptions. The main advantage of assumptions is to simplify the complexity of model developed. To model MSF desalination system, several assumptions were used as described below:

a) Salt free distillate is produced from each stage,
b) Negligible heat of mixing,
c) Generated distillate from previous tray is totally drawn to the product line without entering the next stage,
d) There is no salt accumulation in the tube bundles
e) No sub cooling of condensate leaving the brine heater,
f) No heat losses to the environment (perfect isolation of stages),
g) Flashed vapour has no entrainment of mist.

3.1.2 Model equations

The selected model equations define the overall mass and material balance, energy and enthalpy balances, heat transfer coefficients and physical properties in several units. These units are including individual stage in the heat recovery section and heat rejection stage from stage (1 to j-1), last stage (j), brine heater, MSF seawater splitter, MSF mixer, and demister. More specifically, the model of an individual stage in the two section is also split into flash chamber section, vapour space, distillate tray, and tubes bundle equations. The model equations are presented in Table 2 in the supplementary file.

3.2 Modelling of thermodynamic limitations and exergy analysis of MSF system

The second section of modelling MSF desalination system characterises the exergy analysis and thermodynamic evaluation. Exergy is simply defined as the maximum required work that enables the system to move from an initial state to an environmental state of equilibrium. The total specific exergy (exergy defined by mass flow rate of a selected stream) composes four types of exergy including physical, chemical, potential, and kinetic. However, potential, and kinetic exergies are not important (Mustafa and Al Ghamdi, 2018). This section utilises a set of equations derived from Kahraman and Cengel (2005), and Al-Weshahi et al. (2013). The model equations are given in Table 3 in the supplementary file. In this regard, the physical and chemical exergies are mathematically given in Equations 2, 3, 4 and 9.

The calculations of exergy and overall exergy rate of the Azzour seawater treatment plant are carried out using the model developed in this section that implicitly integrated both physical and chemical exergy analysis.

3.3 Validation of MSF seawater desalination system

The validation of any proposed model is important to appraise its robustness to predict the actual plant data. This section elucidates the validation of the above model. This includes a comparison of the simulation results against the experimental data of Azzour seawater desalination plant. Fig. 2 presents an accurate prediction of the model developed against the actual data of distillate and brine flow rates of Azzour seawater desalination plant. Moreover, Fig. 3 shows the comparison between the simulation results and actual data of pressure and temperature throughout the number of stages of MSF system. Apparently, very marginal errors can be noticed that confidentially reinforce the robustness of the model and therefore the model

will be used to carry out an intensive simulation to evaluate the thermodynamic limitations and exergy analysis of the selected Azzour seawater desalination plant.

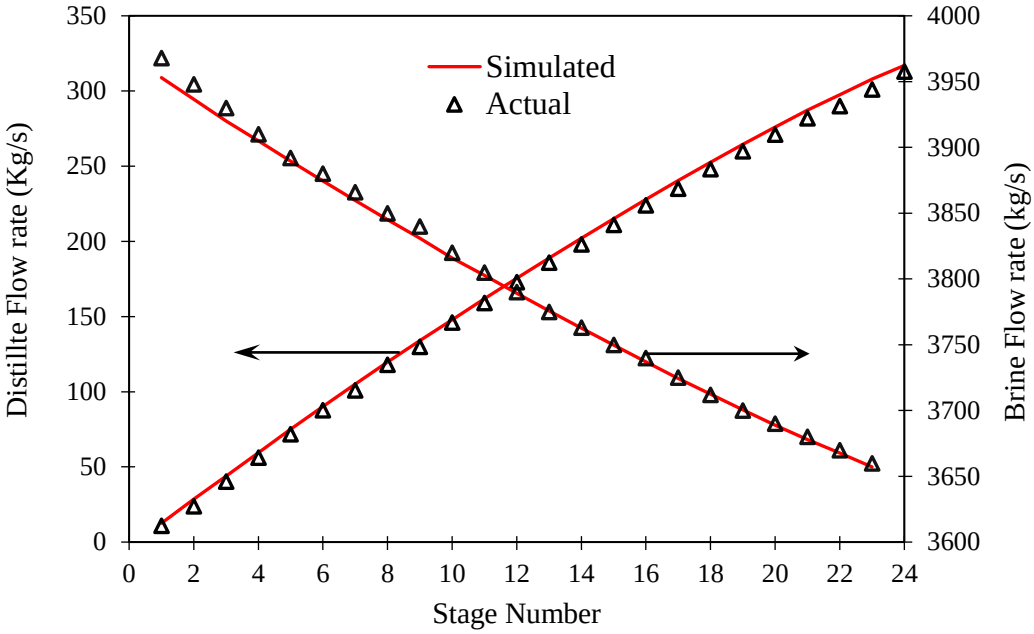

Fig. 2. Comparison of simulation and actual data of distillate and brine flow rates

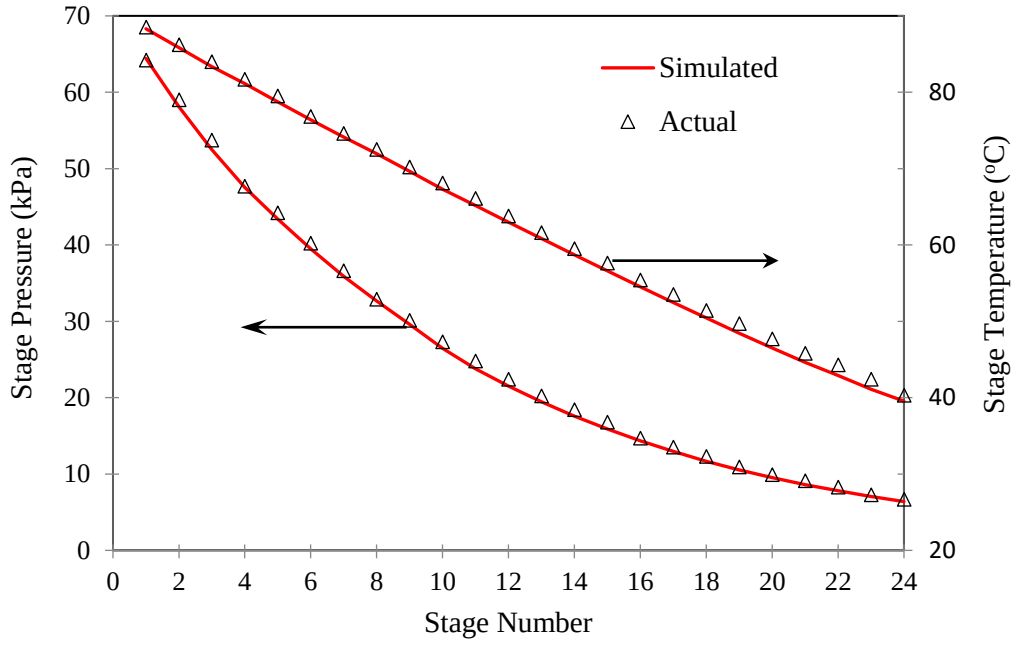

Fig. 3. Comparison between simulation and actual data of stage pressure and temperature

4. Results and Discussion

4.1 Evaluation of thermodynamic limitations and exergy analysis of MSF technology

The exergy analysis of several seawater desalination MSF plants can be found in the literature that examined the possibilities of improving the treatment process. The successful exergy exercise employed to RO process with promising results would stimulate further research on exergy analysis of MSF process with the aim of reducing the total energy consumption and provides a reliable filtration system. The aim of this research is to imperatively tackle with the existed concern of MSF system, particularly Azzour seawater MSF desalination plant, as it represents the most widely used desalination technology in Kuwait. This research therefore intends to critically and thoroughly analyse the exergy losses based on the thermodynamic limitations of the Azzour plant and recommending several options to resolve this challenge.

A detailed schematic diagram of the selected Azzour seawater desalination plant is given in Fig. 1. First, the detailed performance model (presented in Section 3.1) is used to determine the thermodynamic properties of several locations (streams) throughout the MSF system (numbered in Fig. 1) including the temperature, pressure, mass flow rate, and salinity. The simulation results are provided in Table 4. The dead state condition of pressure and temperature are defined as 101.325 kPa and 35 °C, respectively. Second, the model of MSF that incorporated the sub-model of thermodynamic limitations (described in Section 3.2) was used to determine the thermodynamic characteristics in the selected locations (numbered in Fig. 1 and Table 4) throughout the whole MSF plant including the physical and chemical exergies and total exergy for a specified location. Furthermore, the model is then used to measure the exergy of three important sectors of each flashing stage including the input and output streams of condenser, distillate, and brine streams of each flashing stage. More importantly, the calculation of total exergy has included the calculations of physical and chemical exergies that

identified as a strong point of the model used in this study. The thermodynamic properties of seawater cooling inlet to the condensers and seawater cooling outlet from the condensers with exergy calculations of all the corresponding stages (24 stages) are elaborated in Tables 5 and 6, respectively. The thermodynamic properties of collected inlet distillate and outlet distillate with exergy calculations of all the corresponding stages (24 stages) are given in Tables 7 and 8, respectively. The thermodynamic properties of inlet and outlet brine with exergy calculations of all the corresponding stages (24 stages) are given in Tables 9 and 10, respectively. The detailed simulation results of Tables 5 – 10 can be successfully used to assess the destructed exergy for several streams of any stage in the MSF plant.

Table 4. Thermodynamic properties of several locations throughout the Azzour seawater MSF plant and exergy calculations

Location	Mass flow rate (kg/s)	Pressure (kPa)	Salinity (ppm)	Temperature (C)	Physical exergy (kJ/kg)	Chemical exergy (kJ/kg)	Specific exergy (kJ/kg)	Total exergy rate (MW)
0	2674.81	101.32	44000	35	0.00	0.00	0.0000	0.0000
1	2674.81	300	44000	35	0.0002	0.00	0.0002	0.0006
2	2674.81	210	44000	40.29	0.1856	0.00	0.1856	0.4964
3	812.62	210	44000	40.29	0.1856	0.00	0.1856	0.1508
4	812.62	6.84	44000	40.29	0.1854	0.00	0.1854	0.1435
5	315.04	6.84	0	38.12	0.0172	0.00	0.0172	0.0054
6	497.55	6.84	71862.11	39.98	0.4582	2.47	2.9263	1.4560
7	3968.33	6.84	66156.62	39.98	0.3766	1.97	2.3423	9.2952
8	3968.33	712	66156.62	39.98	0.3774	1.97	2.3431	9.2983
9	3968.33	133	66156.62	84.26	14.993	1.33	16.312	64.762
10	3968.33	112	66156.62	90	18.448	1.13	19.577	**77.687**
11	315.04	200	0	38.12	0.0175	0.00	0.0175	0.0055
12	497.55	240	71862.11	39.98	0.4584	2.47	2.9265	1.4561
13	1862.19	210	44000	40.29	0.1856	0.00	0.1856	0.3456
14	39.85	101.325	0	100	487.673	0.0	487.673	19.434
15	39.85	101.325	0	100	34.039	0.0	34.039	1.356

Table 5. Thermodynamic characteristics of inlet cooling seawater with exergy calculations for all the stages

Stage number	Pressure (kPa)	Temperature (°C)	Mass flow rate (kg/s)	Salinity (ppm)	Physical exergy (kJ/kg)	Chemical exergy (kJ/kg)	Exergy (kJ/kg)	Total exergy (MW)
1	60.56	81.75	3968.33	66156.62	13.58	1.407	14.99	59.49
2	54.87	79.22	3968.33	66156.62	12.23	1.483	13.72	54.43
3	49.81	76.69	3968.33	66156.62	10.95	1.554	12.51	49.63
4	44.85	74.18	3968.33	66156.62	9.74	1.619	11.36	45.09
5	40.54	71.70	3968.33	66156.62	8.61	1.679	10.29	40.83
6	36.58	69.23	3968.33	66156.62	7.55	1.732	9.29	36.85
7	32.97	66.80	3968.33	66156.62	6.58	1.780	8.36	33.17
8	29.70	64.41	3968.33	66156.62	5.69	1.822	7.51	29.79
9	26.75	62.09	3968.33	66156.62	4.88	1.857	6.74	26.73
10	24.07	59.85	3968.33	66156.62	4.15	1.887	6.04	23.97
11	21.66	57.66	3968.33	66156.62	3.51	1.912	5.42	21.50
12	19.611	55.54	3968.33	66156.62	2.93	1.932	4.86	19.29
13	17.76	53.49	3968.33	66156.62	2.42	1.948	4.37	17.34
14	16.10	51.53	3968.33	66156.62	1.98	1.959	3.94	15.65
15	14.65	49.64	3968.33	66156.62	1.61	1.967	3.58	14.19
16	13.36	47.82	3968.33	66156.62	1.29	1.972	3.26	12.93
17	12.21	46.08	3968.33	66156.62	1.02	1.975	2.99	11.87
18	11.19	44.42	3968.33	66156.62	0.80	1.975	2.77	10.99
19	10.28	42.85	3968.33	66156.62	0.62	1.973	2.59	10.28
20	9.49	41.38	3968.33	66156.62	0.48	1.970	2.45	9.72
21	8.79	39.99	3968.33	66156.62	0.38	1.966	2.34	9.29
22	8.20	38.53	2674.81	44000	0.08	0.00	0.08	0.214
23	7.55	36.45	2674.81	44000	0.013	0.00	0.013	0.035
24	6.84	35.00	2674.81	44000	0.00	0.00	0.00	0.00

Table 6. Thermodynamic characteristics of outlet cooling seawater with exergy calculations for all the stages

Stage number	Pressure (kPa)	Temperature (°C)	Mass flow rate (kg/s)	Salinity (ppm)	Physical exergy (kJ/kg)	Chemical exergy (kJ/kg)	Exergy (kJ/kg)	Total exergy (MW)
1	60.56	84.26	3968.33	66156.62	14.99	1.327	16.32	**64.76**
2	54.87	81.75	3968.33	66156.62	13.58	1.407	14.99	59.49
3	49.81	79.22	3968.33	66156.62	12.23	1.483	13.72	54.43
4	44.85	76.69	3968.33	66156.62	10.95	1.554	12.51	49.63
5	40.54	74.18	3968.33	66156.62	9.74	1.619	11.36	45.09
6	36.58	71.70	3968.33	66156.62	8.61	1.679	10.29	40.83
7	32.97	69.23	3968.33	66156.62	7.55	1.732	9.29	36.85
8	29.70	66.80	3968.33	66156.62	6.58	1.780	8.36	33.17
9	26.75	64.41	3968.33	66156.62	5.69	1.822	7.51	29.79
10	24.07	62.09	3968.33	66156.62	4.88	1.857	6.74	26.73
11	21.66	59.85	3968.33	66156.62	4.15	1.887	6.04	23.97
12	19.611	57.66	3968.33	66156.62	3.51	1.912	5.42	21.50
13	17.76	55.54	3968.33	66156.62	2.93	1.932	4.86	19.29
14	16.10	53.49	3968.33	66156.62	2.42	1.948	4.37	17.34
15	14.65	51.53	3968.33	66156.62	1.98	1.959	3.94	15.65
16	13.36	49.64	3968.33	66156.62	1.61	1.967	3.58	14.19
17	12.21	47.82	3968.33	66156.62	1.29	1.972	3.26	12.93
18	11.19	46.08	3968.33	66156.62	1.02	1.975	2.99	11.87
19	10.28	44.42	3968.33	66156.62	0.80	1.975	2.77	10.99
20	9.49	42.85	3968.33	66156.62	0.62	1.973	2.59	10.28
21	8.79	41.38	3968.33	66156.62	0.48	1.970	2.45	9.72
22	8.20	40.29	2674.81	44000	0.19	0.00	0.19	0.508
23	7.55	38.53	2674.81	44000	0.08	0.00	0.08	0.214
24	6.84	36.44	2674.81	44000	0.013	0.00	0.013	0.035

Table 7. Thermodynamic characteristics of inlet distillate with exergy calculations for all the stages

Stage number	Pressure (kPa)	Temperature (°C)	Mass flow rate (kg/s)	Physical exergy (kJ/kg)	Exergy (kJ/kg)	Total exergy (MW)
1	60.56	0.00	0.00	0.00	0.00	0.00
2	54.87	85.96	16.91	15.84	15.84	0.2679
3	49.81	83.48	16.94	14.40	14.40	0.2439
4	44.85	80.97	16.86	13.01	13.01	0.2193
5	40.54	78.46	16.70	11.68	11.68	0.1951
6	36.58	75.96	16.51	10.43	10.43	0.1721
7	32.97	73.49	16.32	9.25	9.25	0.1509
8	29.70	71.02	16.03	8.14	8.14	0.1304
9	26.75	68.58	15.64	7.10	7.10	0.1111
10	24.07	66.18	15.19	6.15	6.15	0.0935
11	21.66	63.83	14.66	5.29	5.29	0.0775
12	19.611	61.56	14.22	4.51	4.51	0.0641
13	17.76	59.35	13.76	3.81	3.81	0.0524
14	16.10	57.21	13.32	3.18	3.18	0.0423
15	14.65	55.10	12.65	2.61	2.61	0.0331
16	13.36	53.10	12.15	2.13	2.13	0.0259
17	12.21	51.18	11.68	1.71	1.71	0.0200
18	11.19	49.31	11.14	1.34	1.34	0.0149
19	10.28	47.53	10.62	1.03	1.03	0.0110
20	9.49	45.81	10.00	0.77	0.77	0.0077
21	8.79	44.18	9.39	0.56	0.56	0.0052
22	8.20	42.64	8.82	0.39	0.39	0.0034
23	7.55	41.32	7.53	0.27	0.27	0.0020
24	6.84	39.77	8.88	0.15	0.15	0.0006

Note: Salinity of distillate and chemical exergy are zero

Table 8. Thermodynamic characteristics of outlet distillate with exergy calculations for all the stages

Stage number	Pressure (kPa)	Temperature (°C)	Mass flow rate (kg/s)	Physical exergy (kJ/kg)	Exergy (kJ/kg)	Total exergy (MW)
1	60.56	85.96	16.91	15.84	15.84	0.2679
2	54.87	83.48	16.94	14.40	14.40	0.2439
3	49.81	80.97	16.86	13.01	13.01	0.2193
4	44.85	78.46	16.70	11.68	11.68	0.1951
5	40.54	75.96	16.51	10.43	10.43	0.1721
6	36.58	73.49	16.32	9.25	9.25	0.1509
7	32.97	71.02	16.03	8.14	8.14	0.1304
8	29.70	68.58	15.64	7.10	7.10	0.1111
9	26.75	66.18	15.19	6.15	6.15	0.0935
10	24.07	63.83	14.66	5.29	5.29	0.0775
11	21.66	61.56	14.22	4.51	4.51	0.0641
12	19.611	59.35	13.76	3.81	3.81	0.0524
13	17.76	57.21	13.32	3.18	3.18	0.0423
14	16.10	55.10	12.65	2.61	2.61	0.0331
15	14.65	53.10	12.15	2.13	2.13	0.0259
16	13.36	51.18	11.68	1.71	1.71	0.0200
17	12.21	49.31	11.14	1.34	1.34	0.0149
18	11.19	47.53	10.62	1.03	1.03	0.0110
19	10.28	45.81	10.00	0.77	0.77	0.0077
20	9.49	44.18	9.39	0.56	0.56	0.0052
21	8.79	42.64	8.82	0.39	0.39	0.0034
22	8.20	41.32	7.53	0.27	0.27	0.0020
23	7.55	39.77	8.88	0.15	0.15	0.0006
24	6.84	38.12	9.13	0.06	0.06	0.0002

Note: Salinity of distillate and chemical exergy are zero

Table 9. Thermodynamic characteristics of inlet brine with exergy calculations for all the stages

Stage number	Pressure (kPa)	Temperature (°C)	Mass flow rate (kg/s)	Salinity (ppm)	Physical exergy (kJ/kg)	Chemical exergy (kJ/kg)	Exergy (kJ/kg)	Total exergy (MW)
1	60.56	90.00	3968.33	66156.62	18.45	1.13	19.58	**77.69**
2	54.87	87.49	3951.35	66441.02	16.90	1.24	18.14	71.69
3	49.81	84.97	3934.38	66727.48	15.41	1.35	16.76	65.94
4	44.85	82.44	3917.55	67014.16	13.98	1.46	15.44	60.48
5	40.54	79.91	3900.83	67301.39	12.61	1.56	14.17	55.29
6	36.58	77.39	3884.33	67587.27	11.32	1.66	12.98	50.40
7	32.97	74.88	3868.02	67872.26	10.09	1.75	11.85	45.82
8	29.70	72.40	3852.00	68154.57	8.95	1.84	10.79	41.55
9	26.75	69.95	3836.37	68432.35	7.89	1.92	9.81	37.62
10	24.07	67.56	3821.18	68704.27	6.91	1.99	8.90	34.02
11	21.66	65.23	3806.51	68969.08	6.02	2.06	8.08	30.76
12	19.611	62.96	3792.31	69227.29	5.21	2.12	7.33	27.81
13	17.76	60.75	3778.56	69479.24	4.48	2.17	6.66	25.16
14	16.10	58.60	3765.25	69724.93	3.82	2.22	6.05	22.77
15	14.65	56.54	3752.60	69959.92	3.24	2.27	5.51	20.68
16	13.36	54.55	3740.45	70187.19	2.73	2.30	5.04	18.83
17	12.21	52.62	3728.77	70407.08	2.28	2.34	4.62	17.22
18	11.19	50.78	3717.64	70617.91	1.89	2.36	4.26	15.82
19	10.28	49.01	3707.02	70820.11	1.56	2.39	3.94	14.62
20	9.49	47.34	3697.03	71011.55	1.28	2.41	3.68	13.62
21	8.79	45.76	3687.64	71192.38	1.04	2.42	3.47	12.78
22	8.20	44.27	3678.82	71362.98	0.85	2.44	3.29	12.10
23	7.55	42.99	3671.29	71509.38	0.71	2.45	3.16	11.59
24	6.84	41.48	3662.41	71682.74	0.57	2.46	3.03	11.08

Table 10. Thermodynamic characteristics of outlet brine with exergy calculations for all the stages

Stage number	Pressure (kPa)	Temperature (°C)	Mass flow rate (kg/s)	Salinity (ppm)	Physical exergy (kJ/kg)	Chemical exergy (kJ/kg)	Exergy (kJ/kg)	Total exergy (MW)
1	60.56	87.49	3951.35	66441.02	16.90	1.24	18.14	71.69
2	54.87	84.97	3934.38	66727.48	15.41	1.35	16.76	65.94
3	49.81	82.44	3917.55	67014.16	13.98	1.46	15.44	60.48
4	44.85	79.91	3900.83	67301.39	12.61	1.56	14.17	55.29
5	40.54	77.39	3884.33	67587.27	11.32	1.66	12.98	50.40
6	36.58	74.88	3868.02	67872.26	10.09	1.75	11.85	45.82
7	32.97	72.40	3852.00	68154.57	8.95	1.84	10.79	41.55
8	29.70	69.95	3836.37	68432.35	7.89	1.92	9.81	37.62
9	26.75	67.56	3821.18	68704.27	6.91	1.99	8.90	34.02
10	24.07	65.23	3806.51	68969.08	6.02	2.06	8.08	30.76
11	21.66	62.96	3792.31	69227.29	5.21	2.12	7.33	27.81
12	19.611	60.75	3778.56	69479.24	4.48	2.17	6.66	25.16
13	17.76	58.60	3765.25	69724.93	3.82	2.22	6.05	22.77
14	16.10	56.54	3752.60	69959.92	3.24	2.27	5.51	20.68
15	14.65	54.55	3740.45	70187.19	2.73	2.30	5.04	18.83
16	13.36	52.62	3728.77	70407.08	2.28	2.34	4.62	17.22
17	12.21	50.78	3717.64	70617.91	1.89	2.36	4.26	15.82
18	11.19	49.01	3707.02	70820.11	1.56	2.39	3.94	14.62
19	10.28	47.34	3697.03	71011.55	1.28	2.41	3.68	13.62
20	9.49	45.76	3687.64	71192.38	1.04	2.42	3.47	12.78
21	8.79	44.27	3678.82	71362.98	0.85	2.44	3.29	12.10
22	8.20	42.99	3671.29	71509.38	0.71	2.45	3.16	11.59
23	7.55	41.48	3662.41	71682.74	0.57	2.46	3.03	11.08
24	6.84	39.98	497.56	71862.11	0.46	2.47	2.93	1.46

The results of the Tables 5 – 10 elaborate the calculations of both physical and chemical exergies. In this aspect, it is important to shed a light on the results of the chemical exergy of the brine stream in the flashing stages. The chemical exergy of brine increases due to an increase of salt concentration as the number of stages increases. In other words, the salt content becomes more than the situation of dead state (Tables 9 and 10). Also, the chemical exergy of cooling water in the condensers increases in the heat recovery section as the number of flashing stages increases. In this regard, there is a clear increase of cooling water temperature as it passes from the last stage to the first one. Therefore, this would cause a considerable change (increases) in the physical exergy that dominates the calculations of total exergy for the flashing stage. However, zero chemical exergy for cooling seawater in the heat rejection section is due to the same dead state of salinity (44000 ppm). More importantly, the results of Tables 5 – 10 show that the brine stream has demonstrated the highest exergy destruction and followed by the cooling water stream. However, insignificant values of exergy were registered for the distillate due to the formation of salt free distillate (zero chemical exergy).

The above results of exergy calculations are used to summarise the calculations of total exergy (E_T) of different units of the Azzour MSF plant. This is possible way to differentiate the exergy losses of each unit and specify the main unit that destructing higher exergy. In this aspect, Table 11 demonstrates the applied method to calculate the total exergy. For instance, the total exergy of the heat recovery section comprises the input and output exergies. The recycled brine stream (location 8), the high temperature stream entering the first stage (location 10) are the input streams. The outlet cooling water from the first stage and the outlet high salinity brine from stage 21, and the outlet distillate stream of the stage 21 are represented the outlet streams of the heat recovery section. Similarly, the total exergies of other units are calculated as given in Table 11. Thus, the total percentage contribution of each component is calculated to statistically appraise its influence of the whole destructed exergy of the MSF plant. This is

simply calculated by the division of the total exergy of selected component to the total exergies of all the components in percentage basis. Apparently, the heat recovery section dominates the high destruction of energy as it causes a destruction of exergy of more than 55% from the total destructed exergy of the whole plant. Furthermore, the brine heater is responsible to loss more than 28% of the total exergy due to supplying the cooling seawater with 100 °C. Furthermore, the disposed brine stream and the heat rejection section contribute by around 8% and 5.5% of the total exergy of the plant which are significantly lesser than the exergy of the heat recovery section. On the other hand, the pumping system, which is responsible to pump the feed water inside the system, pumping the recycled stream into the heat recovery section, and withdrawing the product and brine outside the system freshwater stream of the whole plant, represents the lowest destructed exergy. The same trend of these results was affirmed by a comprehensive study of Al-Weshahi et al. (2013) who elaborated that the evaporators of the heat recovery section is responsible to destruct around 54% of the total exergy of an existed MSF plant of capacity of 3800 m^3/h freshwater production. Also, Kempton et al. (2010) and Sharqawy et al. (2011) concluded the same trend of these results.

Table 11. Calculations of total exergy for different units of the Azzour MSF plant

Unit	Location	Applied method	Total exergy (MW)	% Contribution
Destructed Exergy in pumps	-----	$E_T = 0.3333*[(E_{T1} - E_{T0})+(E_{T8} - E_{T7})+(E_{T12} - E_{T6})+(E_{T11} - E_{T5})]$ (Al-Weshahi et al., 2013)	0.0013	0.007
Destructed exergy in brine heater	9 – 10 – 14 – 15	$E_T = (E_{T9} + E_{E14}) – (E_{T10} + E_{T15})$	5.153	28.260
Destructed exergy in the heat recovery stage	----	$E_T = E_{T8} + E_{T10} - E_{T9} - E_{TV21} - E_{TB21}$	10.120	55.500
Destructed exergy in the heat rejection stage	----	$E_T = E_{TB21} + E_{TV21} + E_{T1} + E_{T4} - E_{T2} - E_{T5} - E_{T6} - E_{T7}$	1.001	5.494
Destructed exergy in cooling system of heat rejection section	2	$E_T = E_{T2}$	0.4964	2.722
Destructed exergy of product stream	11	$E_T = E_{T11}$	0.0055	0.030
Destructed exergy of disposed brine stream	12	$E_T = E_{T12}$	1.4561	7.985

4.2 Critical assessment of exergy in the flashing stages

To systematically understand the behaviour of exergy in the three parts of a flashing stage including cooling water, brine and distillate, this section intends to describe the phenomenon inside the flashing stage and its correspondence to destructed exergy. As stated in the Tables 5 – 10, there is a clear reduction of exergy as the number of stages increases. More specifically, the results of the input and output streams of cooling water, brine, and distillate given in Tables 5 – 10 confirm the reduction of exergy as the number of stages increases. This is due to a reduction in the thermal efficiency as the temperature decreases with increasing the number of flashing stages. In other words, the generation of vapour in the prior stages is more than the last stages where the maximum production is entailed at the first stage of the highest operating temperature. Fig. 4 depicts the relationship between the destructed exergy and number of stages in the selected parts of stage.

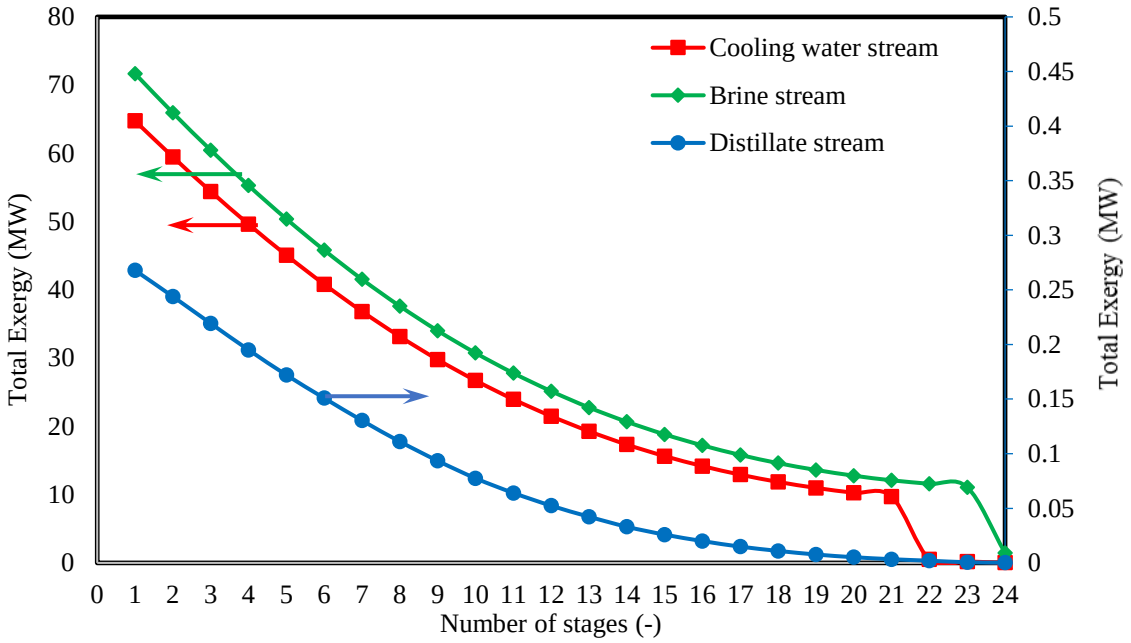

Fig. 4. The exergy profile throughout the flashing stages in heat recovery section and heat rejection section

Fig. 4 and the reported results of Tables 5 – 10 cannot introduce the actual calculations of an individual stage where it is important to consider the exergy for all input and output streams of the corresponding stage. Therefore, Eq. 1 has been demonstrated to quantify the calculation of exergy efficiency of an individual flashing stage as represented below

$$\%Exergy_{stage} = \frac{(E_{T,out} - E_{T,in})_{cooling\ water} + (E_{T,in} - E_{T,out})_{distillate}}{(E_{T,in} - E_{T,out})_{brine}} \quad (1)$$

Thus, a clear view of exergy efficiency of all the stages in the heat recovery section and heat rejection section is demonstrated in Fig. 5. It is essential to realise that attaining the highest exergy efficiency would reflect the most interested aspect where the lowest exergy destruction can be found. Fig. 5 depicts the fact that the exergy efficiency of the stages decreases due to increasing the stage number. In other words, the lowest exergy destruction can be found in the first stage of the maximum exergy efficiency compared to the highest exergy destruction in the last stage of the lowest exergy efficiency. This is clear where 90 °C of top brine temperature at the first stage of the highest thermal load compared to 41 °C at the last stage of the lowest

thermal efficiency. Hence, it is important to maintain higher operating temperature in the flashing stages to guarantee higher performance of exergy efficiency of the flashing stages.

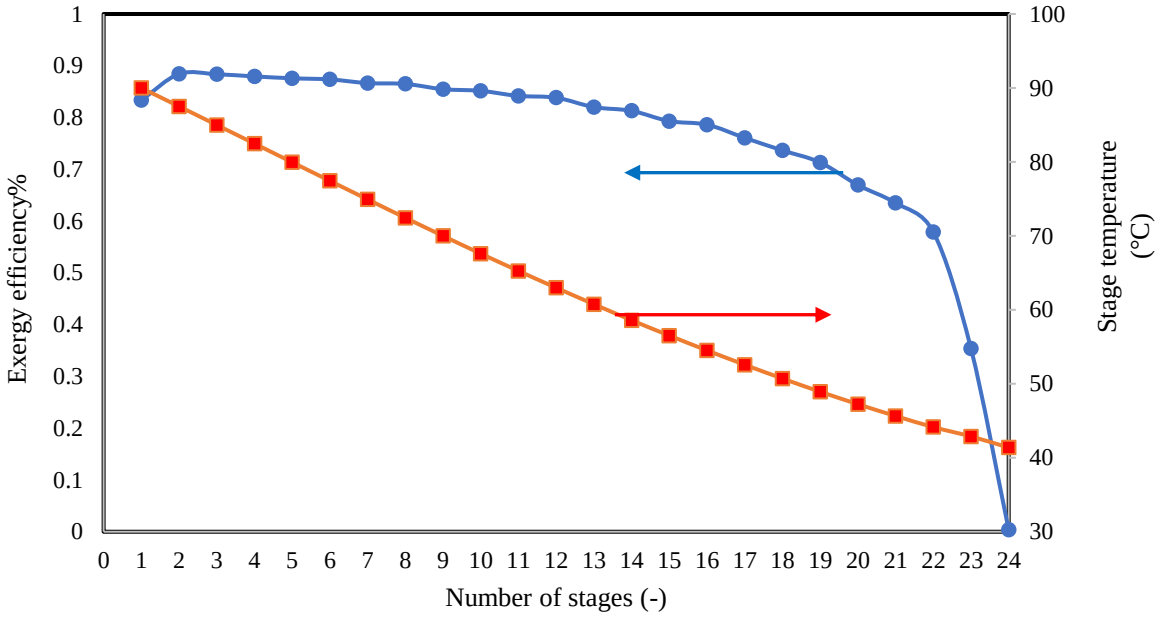

Fig. 5. Exergy efficiency and stage temperature against the number of flashing stages

5. Conclusions

The current research focused on producing a reliable seawater desalination of MSF process of the Azzour desalination plant located in Al Khiran in Kuwait through encountering with concern of exergy destruction. The intention was to explore the thermodynamic limitations of the Azzour seawater desalination that represented the novelty of this research. Therefore, a thermodynamic model was embedded in the performance model that finally constituted a comprehensive model for the MSF process.

Interestingly, the thermodynamic model has ensured the calculations of physical and chemical exergies to demonstrate the total exergy of several locations throughout the Azzour seawater desalination MSF plant. This in turn has enabled to research and analyse the exergy destruction

and determine the most causes of energy losses via simulation-based model of MSF process that coded in gPROMS software suits.

The study explored that the heat recovery section (contains 21 stages) of the Azzour plant is the one responsible with the highest exergy destruction. Statistically, the simulation results confirm that more than 55% of energy is dissipated in the heat recovery section followed by 28% within the brine heater and around 8% and 5.5% within the disposed stream and heat rejection section, respectively, of the MSF plant.

To assess the influence of stage's order of the flashing stages, a critical analysis was carried out and the simulation provided a clear view of the profile of exergy efficiency throughout the stages. Specifically, the last stage has entailed the lowest exergy efficiency compared to the first stage of a maximum efficiency. The high thermal efficiency of the first stage can interpret the main reason. The obtained results of exergy analysis of the Azzour desalination plant agreed the results of other published articles in this topic and therefore suggested to keep research to resolve the current issue via inventing other possible methods of reducing the total energy consumption. However, it is important to admit that the calculations of exergy were carried out under the presumption of ideal solution of seawater, and this might a bit retard the accuracy of the obtained results.

Nomenclature

A_{BH}	Heat transfer surface area of the brine heater (m^2)
As	Heat transfer surface area of a stage (m^2)
B_{in}	Brine inlet flow rate of a stage (kg/s)
B_{out}	Brine outlet flow rate from a stage (kg/s)
BPE	Boiling point elevation (^oC)
B_{vel}	Brine velocity (m/s)
C_1	Correction factor for the number of tubes in vertical direction
C_2	Correction factor for the NCGs)

C_{Be}	Equilibrium mass fraction of NCGs in the brine (ppm)
C_{Bin}	Mass fraction of NCGs in the brine entering a stage (ppm)
C_{Bout}	Mass fraction of NCGs in the brine leaving a stage (ppm)
C_{Fin}	Mass fraction of NCGs entering the HRJ (ppm)
C_{Fout}	Mass fraction of NCGs in the make-up stream (ppm)
C_p	Specific heat at constant pressure (kJ/kg ^oC)
C_{pGas}	Specific heat of NCGs at constant pressure (kJ/kg ^oC)
C_{rec}	Mass fraction of NCGs of the recycle brine (ppm)
C_{VD}	Total condensate flow in a stage (kg/s)
d_i	Inside diameter of tube (m)
d_o	Outside diameter of tube (m)
D_{out}	Distillate flow rate to a stage (kg/s)
D_{total}	Total distillate product flow rate (kg/s)
F_{last}	Sea water makeup entering the last stage (kg/s)
g	Gravity acceleration (m/s^2)
h_b	Height of the brine inside the stage pool (in)
h_i	Brine side heat transfer coefficient ($kW/m^2\ ^oC$)
h_o	Vapour side heat transfer coefficient ($kW/m^2\ ^oC$)
h_s	Total enthalpy of salt
H	Enthalpy of corresponding stream (kJ/kg)
k_B	Brine thermal conductivity (kW/m ^oC)
k_t	Conductivity of the tube material (kW/m ^oC)
k_D	Conductivity of distillate water (kW/m ^oC)
L_t	Tube length of a stage (m)
m_f	Mass flow rate of corresponding stream (kg/s)
MW	Molecular weight (kg/kmole)
NEA	Non-equilibrium allowance (^oC)
N	Number of tubes in vertical direction in the tube bundle
N_t	Number of tubes in the tube bundle
$NCGs$	Non-condensable gases
P	Pressure in a stage (Pa)

PR	Performance ratio (kg Distillate/kg steam)
Q	Heat transferred to cooling brine in a stage (kW)
R	Universal gas constant (J/mole K)
$R_{f,i}$	Internal fouling resistance (m^2 ^oC/kW)
$R_{f,o}$	External fouling resistance (m^2 ^oC/kW)
Rec	Recycle brine flow rate (kg/s)
S	Salt concentration (g/l)
SL_{st}	Chamber load: Brine flow rate per unit length of chamber width (lb/ft hr)
T^*	Temperature reference (^oC)
TBT	Top brine temperature (^oC)
T_{BHin}	Temperature of cooling brine entering brine heater (^oC)
T_{BHout}	Temperature of cooling brine leaving brine heater (^oC)
T_{Bin}	Temperature of flashing brine entering a stage (^oC)
T_{Bout}	Temperature of flashing brine leaving a stage (^oC)
T_{Dout}	Temperature of distillate leaving a stage (^oC)
T_{Fin}	Temperature of cooling brine entering a stage (^oC)
T_{Flast}	Temperature of the sea water makeup entering the last stage (^oC)
T_{Fout}	Temperature of cooling brine leaving a stage (^oC)
T_{NCGs}	Temperature of non-condensable gases (^oC)
T_{NCGsin}	Temperature of non-condensable gases entering a stage (^oC)
$T_{NCGsout}$	Temperature of non-condensable gases leaving a stage (^oC)
T_{steam}	Steam temperature (^oC)
T_{VB}	Temperature of flashed vapour below demister (^oC)
T_V	Temperature of flashed vapour in the vapour space (^oC)
T_{Vin}	Temperature of the vapour entering a stage (^oC)
T_{Vout}	Temperature of the vapour leaving a stage (^oC)
T_w	Tube wall temperature (^oC)
U_{BH}	Overall heat transfer coefficient in the brine heater (kW/m^2 ^oC)
U_o	Overall heat transfer coefficient in a stage (kW/m^2 ^oC)
V_B	Vapour release flow rate from brine in a stage (kg/s)
V_D	Vapour release flow rate from the distillate tray (kg/s)

V_{in}	Vapour flow rate entering a stage (kg/s)
V_{out}	Vapour flow rate leaving a stage (next stage or vent) (kg/s)
W_{cw}	Rejected cooling brine to the sea (kg/s)
W_{BHin}	Brine mass flow rate entering brine heater (kg/s)
W_{BHout}	Brine mass flow rate leaving brine heater (kg/s)
W_{Rin}	Cooling brine flow entering a stage in the HRS (kg/s)
W_{Rout}	Cooling brine flow leaving a stage in the HRS (kg/s)
W_{Fin}	Cooling seawater flow entering a stage in the HRJ (kg/s)
W_{Fout}	Cooling seawater flow leaving a stage in the HRJ (kg/s)
W_{steam}	Steam flow rate (kg/s)
x_s and x_w	Mole fractions of solute and water
x_{s0} and x_{w0}	Mole fractions at dead case.
X	Salt concentration of corresponding stream (ppm)
X_{Bin}	Salt concentration in the brine entering a stage (ppm)
X_{BHin}	Salt concentration in the brine lentering brine heater (ppm)
X_{BHout}	Salt concentration in the brine leaving brine heater (ppm)
X_{Bout}	Salt concentration in the brine leaving a stage (ppm)
X_{rec}	Salt concentration of the recycle brine (ppm)
X_{Rin}	Salt concentration in the cooling brine entering a HRS stages (ppm)
X_{Rout}	Salt concentration in the cooling brine leaving a HRS stages (ppm)
X_{Fin}	Salt concentration in the cooling brine entering a HRJ stages (ppm)
X_{Fout}	Salt concentration in the cooling brine leaving a HRJ stages (ppm)
Y_{in}	Mass fraction of NCGs in the vapour entering a stage (wt. %)
Y_{mole}	Mole fraction of NCGs in the vapour space in a stage (wt. %)
Y_{out}	Mass fraction of NCGs in the vapour leaving a stage (wt. %)

Greek letters

ΔT_B	Brine temperature difference (^oC)
ΔT_{Dem}	Temperature drop through demister (^oC)
ΔP	Pressure difference (Pa)
ρ_B	Brine density (kg/m^3)
ρ_D	Distillate density (kg/m^3)

ρ_V	Vapour density (kg/m^3)
γ	Efficiency of degassing process
λ	Latent heat of vapour in a stage (kJ/kg)
λ_{steam}	Latent heat of steam (kJ/kg)
μ	Viscosity of the fluid (N s/m^2)

References

Abdulrahim H.K., Alasfour F.N., 2010. Multi-Objective Optimisation of hybrid MSF? RO desalination system using Genetic Algorithm. *International Journal of Exergy*, 7(3), 387-424.

Al-Fulaij H.F., 2011. Dynamic modelling of multistage flash (MSF) desalination plant (Doctoral dissertation, UCL (University College London)).

Al-hotmani O.M.A., Al-Obaidi M.A., Patel R., Mujtaba I.M., 2019. Performance analysis of a hybrid system of multi effect distillation and permeate reprocessing reverse osmosis processes for seawater desalination. *Desalination*, 470, 114066.

Alsadaie S.M. Mujtaba I.M., 2016. Generic Model Control (GMC) in Multistage Flash (MSF) Desalination, *Journal of Process Control*, 44, 92–105

Alsadaie S.M., 2017. *Design and Operation of Multistage Flash (MSF) Desalination: Advanced Control Strategies and Impact of Fouling.* Doctoral dissertation, University of Bradford.

Al-Shayji K.A.M., 1998. *Modelling, simulation, and optimization of large-scale commercial desalination plants* (Doctoral dissertation, Virginia Tech).

Alasfour F.N., Abdulrahim H.K., 2009. Rigorous steady state modeling of MSF-BR desalination system. *Desalination and Water Treatment*, 1(1-3), 259-276.

Al-Weshahi M.A., Anderson A., Tian G., 2013. Exergy efficiency enhancement of MSF desalination by heat recovery from hot distillate water stages. *Applied Thermal Engineering*, 53(2), 226-233.

Basile A., Napporn T. eds., 2020. *Current Trends and Future Developments on (Bio-) Membranes: Membrane Systems for Hydrogen Production*. Elsevier.

Bennett A., 2013. 50th Anniversary: Desalination: 50 years of progress. *Filtration+ Separation*, *50*(3), 32-39.

Buabbas S.K., Al-Obaidi M.A., Mujtaba I.M., 2020. A parametric simulation on the effect of the rejected brine temperature on the performance of multieffect distillation with thermal vapour compression desalination process and its environmental impacts. *Asia-Pacific Journal of Chemical Engineering*, 15(6), e2526.

Darwish M.A., 2007. Desalting fuel energy cost in Kuwait in view of $75/barrel oil price. *Desalination*, 208(1-3), 306-320.

El-Dessouky H.T., Ettouney H.M., 2002. *Fundamentals of saltwater desalination*. Elsevier.

Filippini G., Al-Obaidi M.A., Manenti F., Mujtaba I.M., 2019. Design and economic evaluation of solar-powered hybrid multi effect and reverse osmosis system for seawater desalination. *Desalination*, 465, 114-125.

Fitzsimons L., Corcoran B., Young P., Foley G., 2015. Exergy analysis of water purification and desalination: a study of exergy model approaches. *Desalination*, 359, 212-224.

Ghamdi A., Mustafa I., 2016. Exergy analysis of a MSF desalination plant in Yanbu, Saudi Arabia. *Desalination*, 399, 148-158.

Kahraman N., Cengel Y.A., 2005. Exergy analysis of a MSF distillation plant. *Energy Conversion and Management*, 46(15-16), 2625-2636.

Kempton R., Maccioni D., Mrayed S.M., Leslie G., 2010. Thermodynamic efficiencies and GHG emissions of alternative desalination processes. *Water Science and Technology: Water Supply*, 10(3), 416-427.

Mujtaba I.M., Srinivasan R., Elbashir N., eds., *The Water-Food-Energy Nexus: Processes, Technologies and Challenges*, CRC Press, 2017

Mujtaba I.M., Majozi T., Amosa M., eds. *Water Management: Social and Technological Perspectives*, CRC Press, 2018.

Mustafa I., Al Ghamdi,A., 2018. Exergy analysis of thermal seawater desalination—a case study. In Renewable Energy Powered Desalination Handbook (pp. 491-515). Butterworth-Heinemann.

Nafey A.S., Fath H.E.S., Mabrouk A.A., 2006a, Thermo-economic investigation of multi effect evaporation (MEE) and hybrid multi effect evaporation-multistage flash (MEE-MSF) systems, *Desalination*, 201, 241–254.

Nafey A.S., Fath H.E.S., Mabrouk A.A., 2006b. Exergy and thermoeconomic evaluation of MSF process using a new visual package. *Desalination*, 201, 224–240

Ng K.C., Burhan M., Chen Q., Ybyraiykul D., Akhtar F.H., Kumja M., Field R.W., Shahzad, M.W., 2021. A thermodynamic platform for evaluating the energy efficiency of combined power generation and desalination plants. npj Clean Water, 4(1), 1-10.

Sharqawy M.H., Zubair S.M., 2011. On exergy calculations of seawater with applications in desalination systems. *International Journal of Thermal Sciences*, 50(2), 187-196.

UNDESA, 2011. World Urbanization Prospects. The 2011 Revision. https://www.un.org/en/development/desa/population/publications/pdf/urbanization/WUP2011_Report.pdf

Appendix

Table 2. Model equations of the performance prediction model (Alsadaie, 2017)

(1) Modelling of an individual stage from (1 to j-1)	
a) The model equations of flash chamber in each stage ($from\ 1\ to\ j-1$) of the heat recovery section and heat rejection section	
Equation	**Description**
$B_{in} - B_{out} = V_B + NCGs$	To predict the mass flow of the leaving brine
$B_{in}\ X_{Bin} = X_{Bout}\ (B_{in} - V_B - NCGs)$	To predict the brine concentration (X_{Bout}) in the flashing brine
$B_{in}\ C_{Bin} = C_{Bout}\ B_{in} - C_{Bout}\ V_B - NCGs\ (C_{Bout} - 1)$	The non-condensable gases $NCGs$ in the brine
$NCGs = B_{out}\ (C_{Bout} - C_{Be})\ \gamma$	To calculate the stripping rate of $NCGs$. The efficiency of degassing process (γ)
$B_{in}\ C_p\ (T_{Bin} - T^*)\ -\ B_{in}\ C_p\ (T_{Bout} - T^*)\ = V_B\ C_p\ (T_{V_B} - T^*)\ - V_B\ C_p\ (T_{Bout} - T^*) + NCGs\ \ C_p\ (T_{NCGs} - T^*)\ - NCGs\ \ C_p\ (T_{Bout} - T^*)$	The enthalpy balance on the flashing brine of each stage to predict the vapour mass flow rate (V_B) released from brine
$T_B = T_{V_B} + BPE + NEA$	To estimate the brine temperature
b) **The model equations of vapour space in each stage (j) of the heat recovery section and heat rejection section**	
$V_B + V_{in} + V_D + NCGs = C_{VD} + V_{out}$	To calculate the total mass flow rate of condensate (C_{VD}) of produced vapour
$V_{in}\ Y_{in} + NCGs\ (1 - Y_{out}) = Y_{out}\ (V_{in} + V_B + V_D - C_{VD})$	To estimate the non-condensable gases in the vapour space
$V_B\ (C_p\ (T_{VB} - T^*)) + \left(NCGs\ (C_p\ (T_{NCGs} - T^*)\right) + \left(V_{in}\ (1 - Y_{in})\ (C_p\ (T_{Vin} - T^*)\right) + \left(V_{in}\ Y_{in}\ (C_p\ (T_{NCGsin} - T^*)\right) + (V_D\ (C_p\ (T_{Vout} - T^*)) = (C_{VD}\ (C_p\ (T_{VD} - T^*)) + \left(V_{out}\ Y_{out}\ (C_p\ (T_{NCGsout} - T^*)\right) + (V_{out}\ (1 - Y_{out})\ (C_p\ (T_{Vout} - T^*) + Q$	The overall enthalpy balance in the vapour space to estimate the heat transfer rate from the vapour to the condenser tubes to raise the temperature of brine
$T_V = T_{VB} - \Delta T_{DEM}$	To estimate the vapour temperature
c) The model equations of distillate tray in each stage (j) of the heat recovery section and heat rejection section	
$C_{VD} - V_D = D_{out}$	To estimate the total mass flow rate of distillate (D_{out})
$C_{VD}\left((C_p\ (T_{VD} - T^*) - (C_p\ (T_{Dout} - T^*)\right) - V_D((C_p\ (T_{Vout} - T^*) - (C_p\ (T_{Dout} - T^*))$	To predict the total enthalpy balance around the distillate tray
$V_D\ (C_p\ (T_{Vout} - T^*) = C_{VD}\ ((C_p\ (T_{VD} - T^*) - (C_p\ (T_{Dout} - T^*))$	The temperature difference between the vapour in vapour space and distillate
d) The model equations of tubes bundle in each stage (j) of the heat recovery section and heat rejection section are	
$W_{Rin} = W_{Rout}\ ,\ \ W_{Fin} = W_{Fout}$	Total mass balance of tubes bundle in heat recovery and heat rejection sections
$X_{Rin} = X_{Rout},\ \ \ X_{Fin} = X_{Fout}$	The mass balance of tubes bundle in heat recovery and heat rejection sections
$W_{Rin}\ C_p\ (T_{Fout} - T^*) - \ W_{Rin}\ C_p\ (T_{Fin} - T^*) = Q$	The overall enthalpy balance of tubes bundle
$Q = U_o\ A_S\ (\frac{T_{Fout} - T_{Fin}}{\ln\frac{(T_V - T_{Fin})}{(T_V - T_{Fout})}})$	To calculate the supplied heat of steam Q
$A_S = N_t\ \pi\ d_o\ L_t$	To estimate the heat transfer area of the tubes bundle

(2) Modelling of the last stage (j)	
a) The model equations of flash chamber in the last stage (j) of the heat rejection section	
$B_{in} + F_{last} - B_{out} = Rec + V_B + NCGs$	Sea water makeup (F_{last}) and recycle brine flow rate (Rec)
$F_{last} = W_{Fin} - W_{CW},\ Rec = W_{Rin}$	Sea water makeup relates to cooling seawater entering the last stage of heat rejection section and rejected cooling brine mass flow rate disposed to the sea
$B_{in}\ X_{Bin} + Rec\ (X_{Bout} - X_{Rec}) = F_{last}\ (X_{Bout} - X_{Fout}) + X_{Bout}\ (B_{in} - V_B - NCGs)$	Total salt balance of flash chamber of the last stage of heat recovery section
$B_{in}\ C_{Bin} + F_{last}\ (C_{Fout} - C_{Bout}) = Rec\ (C_{Rec} - C_{Bout}) + NCGs\ (1 - C_{Bout}) - C_{Bout}\ (B_{in} - V_B)$	The mass balance of non-condensable gases in the brine
$B_{in}\ C_p\ (T_{Bin} - T^*) - B_{in}\ C_p\ (T_{Bout} - T^*) - F_{Last}\ C_p\ (T_{Bout} - T^*) + F_{Last}\ C_p\ (T_{Flast} - T^*) = V_B\ C_p\ (T_{VB} - T^*) - V_B\ C_p\ (T_{Bout} - T^*) + NCGs\ C_p\ (T_{NCGs} - T^*) - NCGs\ C_p\ (T_{Bout} - T^*)$	The total enthalpy balance
(3) Modelling of the brine heater of the heat recovery section	
$W_{BHin} = W_{BHout},\ X_{BHin} = X_{BHout}$	The total mass and salt balance of brine inside the brine heater.
$W_{BHin}\ C_p\ (T_{BHout} - T^*) - W_{BHin}\ C_p\ (T_{BHin} - T^*) = U_{BH}\ A_{BH}\ (\frac{(TBT - T_{BHin})}{\ln\left[\frac{(T_{steam} - T_{BHin})}{(T_{steam} - TBT)}\right]})$	The total enthalpy balance of the brine heater is based on overall heat transfer coefficient (U_{BH}), total surface of heater (A_{BH}) and logarithmic mean temperature
$U_{BH}\ A_{BH}\ \left(\frac{(TBT - T_{BHin})}{\ln\left[\frac{(T_{steam} - T_{BHin})}{(T_{steam} - TBT)}\right]}\right) = W_{STEAM}\ \lambda_{STEAM}$	To estimate the total heat transfer
(4) Interconnected model of MSF desalination system	
$B_{in\ j} = B_{out\ j-1},\ \ B_{out\ j} = B_{in\ j+1}, T_{Bin\ j} = T_{Bout\ j-1},\ \ T_{Bout\ j} = T_{Bin\ j+1}$ $X_{Bin\ j} = X_{Bout\ j-1}, X_{Bout\ j} = X_{Bin\ j+1},\ C_{Bin\ j} = C_{Bout\ j-1},\ C_{Bout\ j} = C_{Bin\ j+1}$	The total mass and salt balance of brine between the subsequent stages
$V_{in\ j} = V_{out\ j-1},\ V_{out\ j} = V_{in\ j+1},\ \ Y_{in\ j} = Y_{out\ j-1},\ \ Y_{out\ j} = Y_{in\ j+1}$	The total mass balance of vapour and NSGs in the vapour space of the stages.
$W_{Rin\ j} = W_{Rout\ j+1}, W_{Rout\ j} = W_{Rin\ j-1}, T_{Fin\ j} = T_{Fout\ j+1}, T_{Fout\ j} = T_{Fin\ j-1}, X_{Rin\ j} = X_{Rout\ j+1}, X_{Rout\ j} = X_{Rin\ j-1}, C_{Rin\ j} = C_{Rout\ j+1}, C_{Rout\ j} = C_{Rin\ j+1}$	The total mass and salt balance of brine in the tubes bundle of the stages in both heat rejection section and heat recovery section
$Rec\ X_{Rec} + X_{Bout}\ (F_{last} - D_{Total}) = F_{Last}\ X_{Fout} + X_{Bout}\ (Rec - D_{Total})$ $Rec\ C_{Rec} + C_{Bout}\ (F_{last} - D_{Total}) = F_{Last}\ C_{Fout} + C_{Bout}\ (Rec - D_{Total})$	To estimate the recycle brine salinity and NCGs concentration of the last stage of heat recovery section
$Performance\ ratio\ (PR) = \frac{D_{total}}{W_{steam}},\ \ D_{Total} = \sum_{j=1}^{N} D_j$	The total performance ratio and the summation of collected distillate of all stages
$\rho = (A_1\ F_1 + A_2\ F_2 + A_3\ F_3 + A_4\ F_4)\ 10^3$ $A_1 = 4.032219\ G_1 + 0.115313\ G_2 + 3.26\ x10^{-4}\ G_3$ $A_2 = -\ 0.108199\ G_1 + 1.571\ x\ 10^{-3}\ G_2 - 4.23\ x10^{-4}\ G_3$ $A_3 = -\ 0.012247\ G_1 + 1.74\ x10^{-3}\ G_2 - 9\ x10^{-6}\ G_3$ $A_4 = 6.92\ x10^{-4}\ G_1 - 8.7\ x10^{-5}\ G_2 - 5.3\ x10^{-5}\ G_3$ $F_1 = 0.5,\ F_2 = ((2T - 200)/160),\ F_3 = 2\ ((2T - 200)/160)^2 - 1,$ $F_4 = 4\ ((2T - 200)/160)^3 - (3\ ((2T - 200)/160))$ $G_1 = 0.5,\ G_2 = (2X\ /(1000-150)/150),\ G_3 = 2\ ((2X\ /(1000-150)/150))^2 - 1$	The brine density

$\rho_V = \frac{P}{R\,T_V}\,\frac{1}{\left[\left(\frac{(1-Y_{out})}{MW_{H_2O}}\right)+\left(\frac{Y_{out}}{MW_{CO_2}}\right)\right]\times 1000}$	Vapour and gas density.
$C_p = (A + BT + CT^2 + DT^3)x10^{-3}$ $A = 4206.8 - 6.6197\,X + 1.2288\,x10^{-2}\,X^2$ $B = -1.1262 + 5.4178\,x10^{-2}\,X - 2.2719\,x10^{-4}\,X^2$ $C = 1.2026\,x10^{-2} - 5.3566\,x10^{-4}\,X + 1.8906\,x10^{-6}\,X^2$ $D = 6.8777\,x\,l0^{-7} + 1.517\,x10^{-6}\,X - 4.4268\,x10^{-9}\,X^2$	The specific heat capacity of seawater at fixed pressure
$\lambda = 2501.897149 - 2.407064037\,\mathrm{T} + 1.192217x10^{-3}\,T^2 - 1.5863x10^{-5}\,T^3$	The latent heat of water vapour and steam
$\mu = (\frac{\mu_W\,\mu_R}{1000})\,,\ Ln(\mu_W) = -3.79418 + \frac{604.129}{(139.18+T)}\,,\ \mu_R = 1 + A\,X + B\,X^2$ $A = 1.474\,x10^{-3} + 1.5\,x10^{-5}\,T - 3.927\,x10^{-8}\,T^2$ $B = 1.0734\,x10^{-5} - 8.5\,x10^{-8}\,T + 2.23\,x10^{-10}\,T^2$	The dynamic viscosity of seawater
$BPE = A\,X + B\,X^2 + C\,X^3$ $A = (8.325\,x10^{-2} + 1.883\,x10^{-4}\,T + 4.02\,x10^{-6}\,T^2)$ $B = (-7.625\,x10^{-4} + 9.02\,x10^{-5}\,T - 5.2\,x10^{-7}\,T^2)$ $C = (1.522\,x10^{-4} - 3\,x10^{-6}\,T - 3\,x10^{-8}\,T^2)$	The boiling point elevation of seawater
$NEA = \frac{195\,h_b{}^{1.1}\left(SL_{st}\,x10^{-3}\right)^{0.5}}{(\Delta T_B)^{0.25}\ (T_V)^{2.5}}$	To estimate the Non-equilibrium allowance (NEA)
$\Delta T_{Dem} = \frac{[EXP(1.885 - 0.02063\,T_{Dout})]}{1.8}$	The temperature drop (ΔT_{Dem})
$LOG\ P(1 - Y_{mole}) = 23.2256 - \left(\frac{3835.18}{T_V + 45.343}\right)$	To estimate the saturation pressure (P)
$Log_{10}(k_B) = Log_{10}(240 + 2\times 10^{-4}\,X) + 0.434\left(2.3 - \frac{343.5+3.7\times 10^{-2}\,X}{T_{Bout}+273.15}\right)\left(1 - \frac{T_{Bout}+273.15}{647.3\times 3\times 10^{-2}\,X}\right)^{1/3}$	The thermal conductivity of seawater
$\frac{1}{U_o} = \left(\frac{d_o}{h_i\,d_i}\right) + \left(R_{fi}\,\frac{d_o}{d_i}\right) + \left(\frac{d_o}{2k_t}\right) Ln\left(\frac{d_o}{d_i}\right) + R_{fo} + \left(\frac{1}{h_o}\right)$	To predict the overall heat transfer coefficient
$h_i = \frac{\left((3293.5 + T_{Fout}\,(84.24 - 0.1714\,T_{Fout}) - X\,(8.471 + 0.1161\,X + 0.2716\,T_{Fout})\right)}{\left(\left(\frac{d_i}{0.017272}\right)^{0.2}\right)((0.656 B_{vel})^{0.8})\left(\frac{d_i}{d_o}\right)}$ $h_o = 0.725\left[\frac{g\,k_D{}^3\rho_D(\rho_D - \rho_v)\,\lambda}{\mu\,d_o(T_{Dout} - T_w)}\right]^{0.25} C_1\,C_2$ $C_1 = 1.23795 + 0.353808\,N - 0.0017035\,N^2$ $C_2 = 1.0 - 34.313\,Y_{out} + 1226.8\,Y_{out}^2 - 14923\,Y_{out}^3$	To estimate the internal heat transfer coefficient (h_i) for brine and external heat transfer coefficient (h_o) for vapour
$N = 0.564\sqrt{\frac{4W_{Rout}}{\pi {d_i}^2 \rho_B B_{vel}}}$	To estimate the number of tubes bundle
$H_V = 2501.689845 + 1.806916\,T + 5.0877x10^{-4}\,T^2 - 1.122x10^{-5}\,T^3$ $H_D = -0.033635 + 4.207557\,T - 6.2x10^{-4}\,T^2 + 4.45937x10^{-6}\,T^3$ $H_{NCGs} = Cp_{Gas}\,(T - T^*)$	The enthalpy of vapour, distillate and NCGs

Table 3. Model equations of the thermodynamic limitations and exergy analysis (Kahraman and Cengel, 2005; Al-Weshahi et al., 2013)

No.	Equation	Description
1	$M_s = \frac{salinity_{PPM}}{10^6}, \quad M_w = 1 - M_s$	To predict the salt (M_s) and water (M_w) mass fractions of a specified stream
2	$e^t = e^{ph} + e^{ch}$	The total limited specific exergy including the physical and chemical exergies
3	$e^{ph} = m_f \, T_o \, R \left[(x_s \log\left(\frac{x_s}{x_{s0}}\right) + (x_w \log\left(\frac{x_w}{x_{w0}}\right) \right]$	e^{ph} relates to mixing effect
4	$e^{ph} = (h - h_o) - T_o \, (s - s_o)$	e^{ph} relates temperature and pressure effects
5	$h_s = h_w - M_s[(-2.348E4) + 3.152E5 \, M_s + 2.803E6 \, {M_s}^2 + (-1.446E7) \, {M_s}^3 + 7.826E3 \, T + (-4.417E1) \, T^2 + 2.139E-1 \, T^3 + (-1.991E4) \, M_s \, T + (2.778E4) \, {M_s}^2 \, T + 9.728E1 \, M_s \, T^2]$	The total enthalpy of salt (h_s)
6	$h_w = 141.355 + 4202.07 \, T - 0.535 \, T^2 + 0.004 \, T^3$	The total enthalpy of water (h_w)
7	$s_s = s_w - M_s[(-4.231E2) + 1.463E4 \, M_s + (-9.88E4) \, {M_s}^2 + (3.095E5) \, {M_s}^3 + 2.562E1 \, T + (-1.443E-1) \, T^2 + (5.879E-4) \, T^3 + (-6.111E1) \, M_s \, T + 8.041E1 \, {M_s}^2 T + 3.035E-1 \, M_s \, T^2]$	The entropy of salt (s_s)
8	$s_w = 0.1543 + 15.383 \, T - 2.996E-2 \, T^2 + 8.193E-5 \, T^3 - 1.37E-7 \, T^4$	The entropy of water (s_w)
9	$e^{ch} = M_s \, (\mu_s - \mu_{s0}) + M_w \, (\mu_w - \mu_{w0})$	To calculate the chemical exergy of a mixture
10	$\mu_s = (h_s - (T \, s_s)) + (M_w \left[\left(\frac{\partial h_s}{\partial M_s}\right) - T \left(\frac{\partial s_s}{\partial M_s}\right) \right])$	The chemical potential of salt
11	$\mu_w = (h_s - (T \, s_s)) + (M_s \left[\left(\frac{\partial h_s}{\partial M_s}\right) - T \left(\frac{\partial s_s}{\partial M_s}\right) \right])$	The chemical potential of water
12	$\left(-\frac{\partial h_s}{\partial M_s}\right) = (-2.348E4) + (2x3.152E5 \, M_s) + (3x2.803E6 \, {M_s}^2) + (-4x1.446E7) \, {M_s}^3 + 7.826E3 \, T + (-4.417E1) \, T^2 + 2.139E-1 \, T^3 + (-2x1.991E4) \, M_s \, T + (3x2.778E4) \, {M_s}^2 \, T + (2x9.728E1 \, M_s \, T^2)$	Enthalpy of salt

13	$\left(-\frac{\partial s_s}{\partial M_s}\right) = (-4.231E2) + (2x1.463E4)M_s + (-3x9.88E4)\ {M_s}^2 + (4x3.095E5)\ {M_s}^3 + 2.562E1\ T + (-1.443E-1)\ T^2 + (5.879E-4)\ T^3 + (-2x6.111E1)\ M_s\ T + (3x8.041E1)\ {M_s}^2 T + (2x3.035E-1)\ M_s\ T^2$	Entropy of salt
14	$eff = \frac{W_{min}}{E_{input}}$	The exergy efficiency
15	$eff_{stage} = \frac{(E_{out} - E_{in})_{cooling} + (E_{in} - E_{out})_{distillate}}{(E_{in} - E_{out})_{brine}}$	The exergy efficiency of each stage